ACS OMEGA

http://pubs.acs.org/journal/acsodf

Article

A Facile and Reproducible Synthesis of Near-Infrared Fluorescent Conjugates with Small Targeting Molecules for Microbial Infection Imaging

Friederike Reeßing, Mafalda Bispo, Marina López-Álvarez, Marleen van Oosten, Ben L. Feringa, Jan Maarten van Dijl, and Wiktor Szymański*

Cite This: *ACS Omega* 2020, 5, 22071−22080

Read Online

ACCESS | Metrics & More | Article Recommendations | Supporting Information

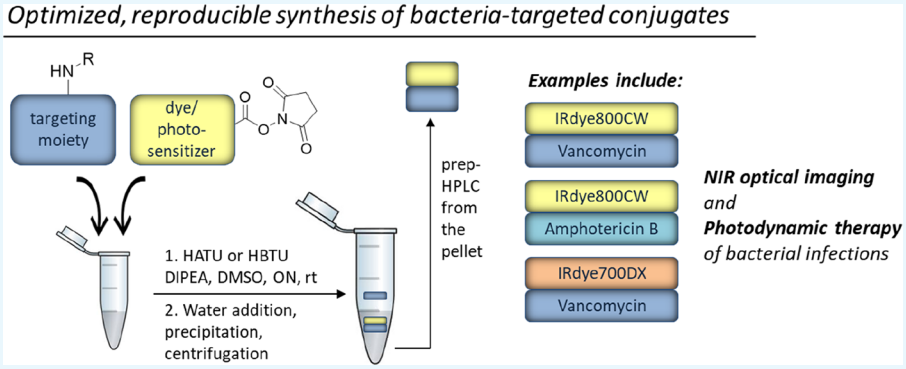

ABSTRACT: Optical imaging of microbial infections, based on the detection of targeted fluorescent probes, offers high sensitivity and resolution with a relatively simple and portable setup. As the absorbance of near-infrared (NIR) light by human tissues is minimal, using respective tracers, such as IRdye800CW, enables imaging deeper target sites in the body. Herein, we present a general strategy for the conjugation of IRdye800CW and IRdye700DX to small molecules (vancomycin and amphotericin B) to provide conjugates targeted toward bacterial and fungal infections for optical imaging and photodynamic therapy. In particular, we present how the use of coupling agents (such as HBTU or HATU) leads to high yields (over 50%) in the reactions of amines and IRDye-NHS esters and how precipitation can be used as a convenient purification strategy to remove excess of the targeting molecule after the reaction. The high selectivity of the synthesized model compound Vanco-800CW has been proven *in vitro*, and the development of analogous agents opens up new possibilities for diagnostic and theranostic purposes. In times of increasing microbial resistance, this research gives us access to a platform of new fluorescent tracers for the imaging of infections, enabling early diagnosis and respective treatment.

INTRODUCTION

Molecular imaging[1−4] plays a crucial role in modern medicine, and several imaging methods are routinely applied in the clinic for diagnosis and monitoring of disease progression and treatment efficacy or for guiding surgical interventions. These methods include tomographic imaging, e.g., magnetic resonance imaging (MRI), positron emission tomography (PET), or computed tomography (CT), which offer the advantage of whole-body imaging but are limited by different factors, like poor temporal resolution due to post-acquisition image reconstruction, application of hazardous radiation (PET), or limited choice of targeted contrast agents (CT and MRI).[5] Conversely, fluorescence-based optical imaging overcomes these drawbacks by enabling real-time, high-resolution visualization in the absence of damaging radiation. Moreover, it stands out due to its economical and straightforward usage.[6]

Optical imaging (OI) relies on the detection of fluorescent probes after their excitation with light of an appropriate wavelength using a fluorescence camera.[7] However, absorption and scattering of the excitation and emitted light in biological tissues limit the possible imaging depth.[8] Since these effects are less pronounced for red or near-infrared (NIR) light, the development of respective dyes enhances the imaging depth and has led to the successful use of OI for different applications, such as image-guided surgery,[9−13] endos-

Received: May 6, 2020
Accepted: August 11, 2020
Published: August 26, 2020

https://dx.doi.org/10.1021/acsomega.0c02094
ACS Omega 2020, 5, 22071−22080

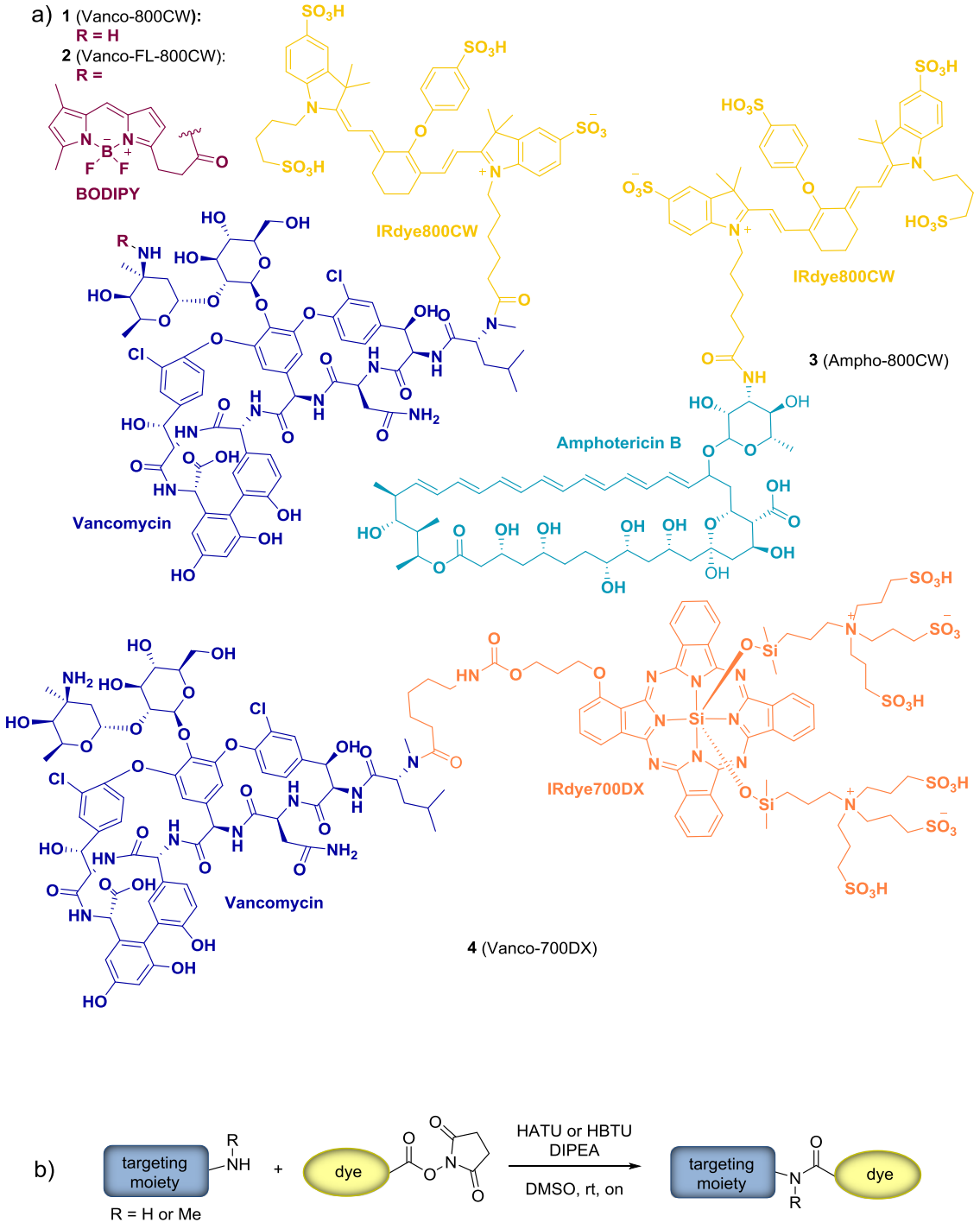

Figure 1. (a) Molecular structures of the synthesized targeted optical imaging agents: Vanco-800CW (**1**), Vanco-FL-800CW (**2**), Ampho-800CW (**3**), and Vanco-700DX (**4**). (b) General synthetic procedure.

copy,[14−16] and pathology.[17−19] The first clinically approved NIR dyes[20] were indocyanine green (ICG) and methylene blue (MB), but a variety of molecules and nanoparticles are currently being tested in clinical studies to implement agents with improved absorptivity or fluorescence quantum yields at even higher wavelengths or targeted agents, enabling selective imaging of important biomarkers.[10,14,21−24] Among those, the NIR dye IRdye800CW[25−30] has shown great promise in clinical translation.

IRdye800CW shows a sharp absorption band at λ_{max} = 774−778 nm, high fluorescence quantum yield,[5] and low nonspecific binding to cellular components.[31] It is mostly applied for the creation of targeted OI agents in which it is conjugated to molecules that enable its selective accumulation at the disease spot. This is most prominently exemplified by proteins. Different antibody-IRdye800CW conjugates show truly promising results in clinical studies for intraoperative imaging.[19]

While the conjugation to macromolecules has been thoroughly researched and optimized,[1] the coupling to small molecules is still rather unexplored. However, synthetic accessibility, stability, and lower price are substantial

https://dx.doi.org/10.1021/acsomega.0c02094
ACS Omega 2020, 5, 22071−22080

Table 1. Screened Reaction Conditions for the Synthesis of Conjugate 1[a]

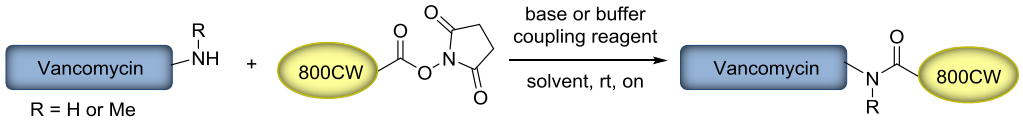

entry	solvent(s)	pH/base	equivalents of vancomycin	coupling reagent	conversion[b]
1	DMSO	DIPEA	2.4		
2	DMSO/phosphate buffer (20 mM)	>7.3	2.4		
3	DMSO/phosphate buffer (20 mM)	6.5−7	12.4		<10%
4	DMSO/phosphate buffer (10−1000 mM)	6.95	2.4−24.7		<10%
5	DMSO	DBU (5−13 eq)	13		
6	DMSO	DIPEA (13 eq)	13	EDC or DIC	
7	DMSO	DIPEA (13 eq)	13	HATU or HBTU	50 −73%
8	DMSO	DIPEA (13 eq)	13	HOBt	11%

[a]Entry 1 presents the published conditions.[39] The reaction medium (DMSO/phosphate buffer), the base, and equivalents of vancomycin and additives were varied, leading to entry 7 as the optimized conditions. [b]The conversion to product **1** was assessed by analysis of the HPLC trace recorded at 760 nm (see the Supporting Information for details).

advantages of small molecules as targeting moieties. This is further highlighted by their capacity to provide well-defined molecular architectures of the final luminescent conjugates due to the limited number of possible conjugation sites.[32] However, the reports on small molecule-IRDye800CW conjugates are scarce, and they involve usually simple molecules, such as vorinostat,[33] 2-deoxyglucose,[34] NOTA chelator,[35] prostate-specific membrane antigen ligands,[36,37] and simple peptides.[38] To the best of our knowledge, there is only one report describing a targeted small molecule-IRdye800CW conjugate for OI that would use a multifunctional structure as a starting point, namely, vancomycin-IRDye800CW (Vanco-800CW). This molecule was designed and evaluated for the imaging of infections with Gram-positive bacteria, showing that it is possible to label the antibiotic vancomycin without abolishing the binding affinity to its bacterial target.[39]

General challenges in labeling small molecules with IRdye800CW are the control over the selectivity of modification in a complex molecular context of the target molecule and the need for nonstandard reaction conditions and purification methods due to the high polarity of the dye. To facilitate the development of conjugates for OI, we introduce here an optimized procedure for the synthesis and facile purification of small molecule conjugates of IR-dye800CW, taking Vanco-800CW (compound **1**) as a reference compound and expanding it toward other small molecule targets and dyes (compounds **2**−**4**; Figure 1), which are potential fluorescent tracers for bacterial (**2**) and fungal (**3**) infections and antimicrobial photodynamic therapy (aPDT) agents (**4**). Moreover, we provide a thorough analysis of the synthesized conjugates, revealing a revised structure for Vanco-800CW.

RESULTS AND DISCUSSION

With the aim to establish a synthetic method for conjugation of IRdye800CW and related IR dyes with small targeting molecules, which could be easily performed in a standard (bio-) chemistry lab, we started by exploring the published procedure for the coupling of IRdye800CW-NHS ester with vancomycin.[39] We were particularly interested in establishing reaction conditions that are easily reproducible also on a small scale since often only minimal amounts of the respective products are required for, e.g., screening of different conjugates, and the dye molecules are generally quite expensive. The published method describes the synthesis of Vanco-800CW from IRdye800CW-NHS ester and vancomycin hydrochloride hydrate in the presence of *N*,*N*-diisopropylethylamine (DIPEA) in DMSO. The use of organic solvent ensures the solubility of both the dye and the final conjugate. Furthermore, the primary amine of vancomycin has been proposed as the conjugation site, while it is important to point out the presence of a secondary amine that could also potentially act as a nucleophile in the reaction with IRdye800CW-NHS ester (*vide infra*). Unfortunately, in our hands, the reported procedure did not yield the desired compound but resulted in hydrolysis of the NHS ester (Table 1, entry 1). A possible explanation for this outcome is the presence of water in DMSO since already small amounts can cause hydrolysis, and we did not take additional precautions to assure dry reaction conditions. Inspired by conditions optimized for labeling antibodies with IRdye800CW-NHS ester,[40] we explored how the reaction proceeds in phosphate buffer at different pH values (Table 1, entries 2 and 3). The data presented in Table 1 shows that, at pH > 7.3, hydrolysis is the prevalent process and no product is formed. In contrast, the reaction in a buffered medium at pH 6.5−7 gave conversion to **1** but in a low yield. Aiming to improve this result, we assessed the influence of different buffer strengths and equivalents of vancomycin on the reaction outcome (Table 1, entry 4). It is important to note that the cost of the dye exceeds that of the antibiotic by several orders of magnitude, which motivates the use of the latter in excess to promote the conjugation. It was found that addition of ca. 13 eq of vancomycin boosts conversion, but additional escalation did not improve it further. Likewise, different buffer strengths did not have any significant effects on the product formation. Under all conditions tested, hydrolysis of the NHS ester to the free acid was the competing reaction.

To tackle this problem, we screened different coupling reagents that would facilitate the formation of the desired amide bond from the acid liberated upon hydrolysis (Table 1, entries 6−8).[41] Addition of the commonly used carbodiimide-based coupling reagents 1-ethyl-3-(3-dimethylaminopropyl)-carbodiimide (EDC) and *N*,*N*′-diisopropylcarbodiimide (DIC) to the reaction mixture containing the substrates and DIPEA in DMSO did not lead to the desired result (Table 1, entry 6), whereas 1-[bis(dimethylamino)methylene]-1*H*-1,2,3-

https://dx.doi.org/10.1021/acsomega.0c02094
ACS Omega 2020, 5, 22071−22080

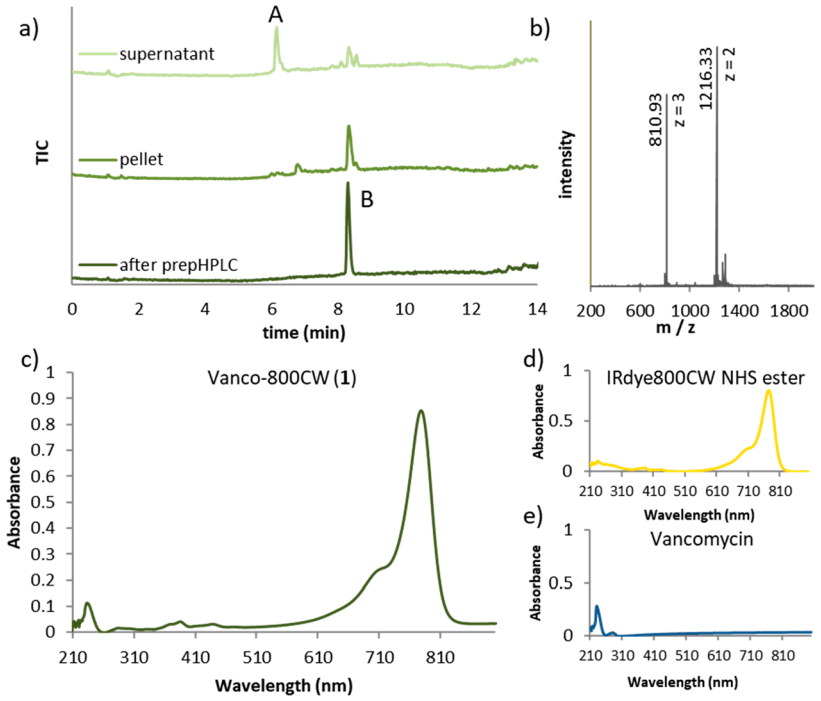

Figure 2. Analytical data for the synthesis and evaluation of Vanco-800CW (**1**). (a) UPLC-MS traces (TIC), collected after addition of water to the reaction mixture, of the supernatant (top), pellet (middle), and HPLC-purified product (bottom). Peak A corresponds to vancomycin, and peak B corresponds to Vanco-800CW. (b) Mass spectrum corresponding to Vanco-800CW (compound **1**, peak B from panel a). (c) UV−vis absorption spectra for Vanco-800CW (**1**), (d) IRdye800CW NHS ester, and (e) vancomycin hydrochloride (2.8 μM, 1% DMSO in water). In panel (c), distinct bands at λ_{max} = 776 and 232 nm are observed, which are also present in the spectrum of IRdye800CW NHS ester (λ_{max} = 776 nm, spectrum d) and vancomycin (λ_{max} = 232 nm, spectrum e).

triazolo[4,5-b]pyridinium 3-oxide hexafluorophosphate (HATU) or (2-(1*H*-benzotriazol-1-yl)-1,1,3,3-tetramethyluronium hexafluorophosphate (HBTU) successfully provided up to 73% conversion to **1** (Table 1, entry 7). Interestingly, we observed that the already hydrolyzed NHS ester was not consumed in the course of the reaction. Furthermore, we did not observe the formation of the vancomycin dimer, which could emerge as a result of the reaction of the amine group in one antibiotic molecule with the coupling agent-activated carboxylic group in another molecule. Accordingly, HATU and HBTU did not seem to function as coupling reagents but rather to promote the product formation in a different manner. In contrast to EDC and DIC, HATU and HBTU comprise a 1-hydroxybenzotriazole (HOBt) moiety, which is known to act as a nucleophilic catalyst for acyl transfer reactions.[41] Therefore, we were curious to explore the effect of using only HOBt in the conjugation reaction (Table 1, entry 8). Remarkably, HOBt did not promote amide formation to the same extent. Considering these results, we attribute the efficient formation of the product in the HATU- and HBTU-mediated reactions to their solvent drying effect, which minimizes the competing hydrolysis of the NHS ester and favors the conversion to the product. We have further established that, in those reactions, the order of addition of the reactants does not influence the reaction outcome and no special instrumental setup or expensive nonstandard chemicals are required. Moreover, it should be emphasized that the reaction does not need to be carried out under strict anhydrous conditions, making this procedure easily reproducible. It has to be noted, however, that substrate concentration plays an important role and dilution of the reaction mixture substantially slows down the chemical conversion (see below).

Next, we proceeded with the purification of compound **1**. The method of choice for such highly complex and polar compounds is usually the purification by (semi-) preparative reversed-phase high-performance liquid chromatography (HPLC), which is often very inefficient regarding time and isolated yields. Hence, we were pleased to achieve a first and straightforward purification step by addition of an excess of water to the reaction mixture, resulting in the precipitation of the conjugate, while most of the vancomycin used in excess in the reaction remained in the solution (Figure 2). This measure allowed a much more efficient removal of the remaining impurities by semipreparative HPLC. Subsequently, the newly synthesized Vanco-800CW was analyzed by ultraperformance liquid chromatography−mass spectrometry (UPLC-MS) and UV−vis spectrometry to assess its purity and identity, as illustrated in Figure 2.

The molecular structure of vancomycin bears two amine functionalities—a primary one on the sugar moiety and a secondary one at the peptide *N*-terminus—that could possibly undergo the reaction with an NHS ester to form an amide (Figure 3a). Generally, coupling to the secondary amine is more efficient[42] due to its higher nucleophilicity. Moreover, the fact that the primary amine is positioned at a tetra-substituted carbon atom increases steric hindrance and thus impedes reaction at this position. To assess which amine reacts to form the conjugate, we investigated the identity of the synthesized product **1** using high-resolution tandem mass spectrometry (HRMS-MS) (Figure 3b). Remarkably, the detected fragments correspond to Vanco-800CW after the loss of one or both sugar moieties, revealing that the dye is coupled to the secondary amine instead of the primary one, as opposed to what was suggested in the earlier report.[39]

https://dx.doi.org/10.1021/acsomega.0c02094
ACS Omega 2020, 5, 22071−22080

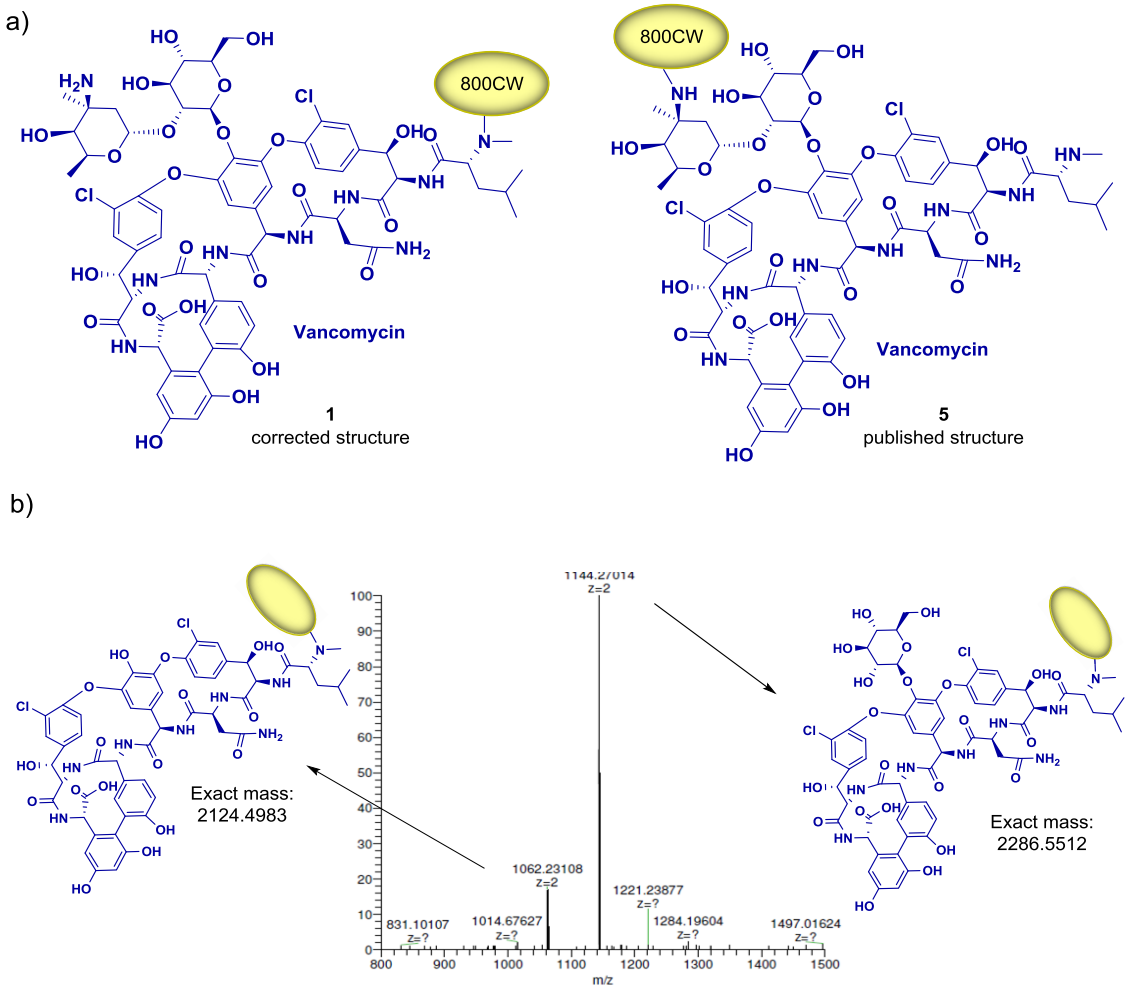

Figure 3. Structure determination of **1**. (a) Molecular structure of synthesized compound **1** and of Vanco-800CW published in the literature.[39] (b) Fragment ions detected by HRMS-MS correspond to the conjugate of IRdye800CW with vancomycin after loss of one or both sugar moieties.

Importantly, the fragmentation that leads to the loss of sugar units in tandem MS is a common phenomenon, often applied in oligosaccharide sequence analysis.[43] It remains unclear what the exact structure of the originally published compound is due to lacking access to respective analytical data and the fact that small changes in reaction conditions may influence the regioselectivity, as shown in an early publication by Staroske and Williams.[44] Of note, an alternative strategy for precise labeling of vancomycin for imaging purposes, which relies on the thiol−maleimide reaction, has been published recently.[45]

With the purified conjugate in hand, we performed a biological evaluation to confirm that the newly synthesized regioisomer of **1** shows the same binding affinity toward Gram-positive bacteria as the earlier reported conjugate. Staphylococcal biofilms, composed of either a *Staphylococcus aureus* clinical isolate or *Staphylococcus epidermidis* ATCC, were established on the surface of 18 mm chemically resistant borosilicate glass coverslips. *Escherichia coli* ATCC was used as a Gram-negative control since vancomycin is known to target only Gram-positive bacteria.[39] The biofilms were then incubated with Vanco-800CW, and images were acquired with a fluorescence microscope. As shown in Figure 4a, Vanco-800CW is capable of binding to both *S. aureus* and *S. epidermidis* with similar affinity. As predicted, no binding was observed to *E. coli*, supporting the view that vancomycin modified with the IRdye800CW retains its binding selectivity and molecular target. Moreover, a control experiment with *S. epidermidis* showed that the IRdye800CW-carboxylic acid without a targeting moiety does not bind to Gram-positive bacteria, excluding the unselective staining (Figure S17).

With the aim to broaden the applicability of the targeted tracer, we proceeded with the synthesis of a dual-labeled vancomycin, starting from commercially available vancomycin BODIPY-FL (Vanco-FL). This probe bears a fluorescent BODIPY moiety on the primary amine, which absorbs light of λ = 505 nm and emits at λ = 512 nm. Even though this wavelength range is not in the optimal window as explained earlier, functionalizing it with an NIR fluorescent moiety opens up new possibilities to use one single probe for multimodal imaging and theranostic approaches (e.g., coupling of Vanco-FL to a photosensitizer for the diagnosis of bacterial infections and subsequent eradication with antimicrobial photodynamic therapy). Toward this end, we reacted Vanco-FL with the IRdye800CW-NHS ester as a model dye using the standard conditions established before for the synthesis of Vanco-800CW. Due to the limited availability of Vanco-FL, we used less equivalents of vancomycin (5 eq compared to 13 eq used before) and a lower substrate concentration, which resulted in longer reaction times with ca. 60% conversion to the product after 5 days (Figure S4). The successful formation of the desired dual-labeled vancomycin (**2**, Vanco-FL-800CW; Figure 1) was confirmed by UPLC-MS and analysis of the UV−vis

https://dx.doi.org/10.1021/acsomega.0c02094
ACS Omega 2020, 5, 22071−22080

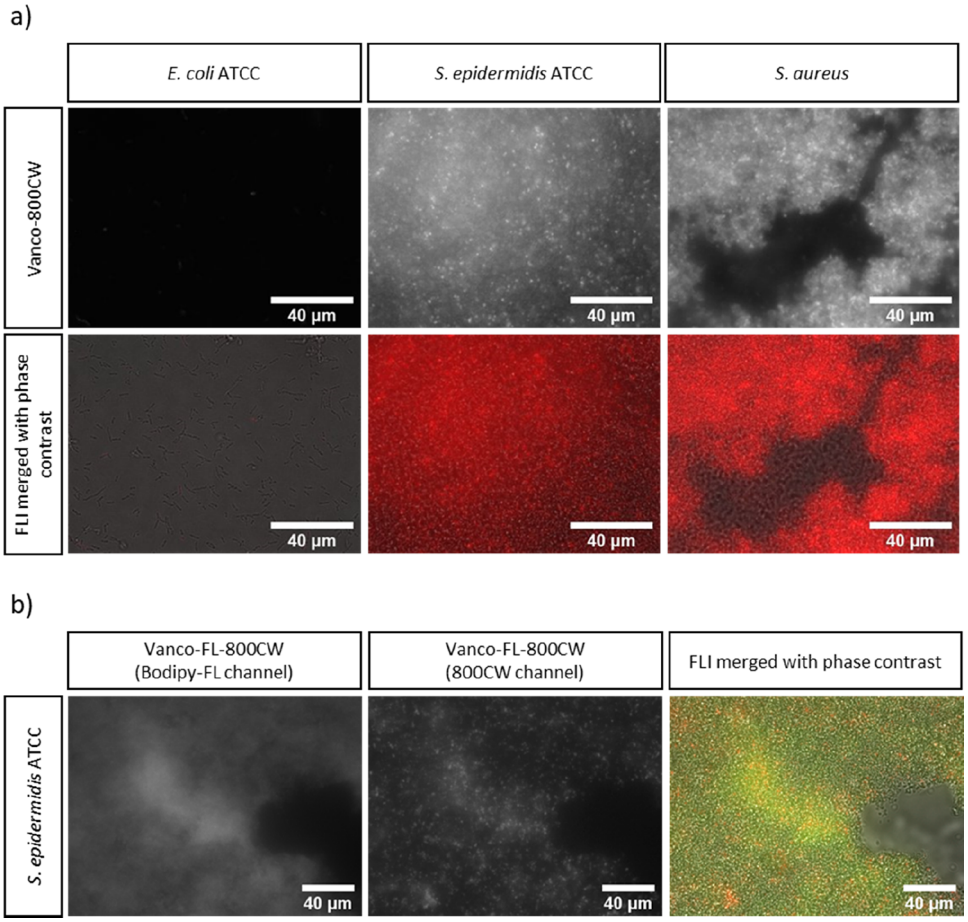

Figure 4. *In vitro* detection of bacterial biofilms using the (a) Vanco-800CW and (b) Vanco-FL-800CW probes. (a) Biofilms of *S. aureus*, *S. epidermidis* ATCC, or *E. coli* ATCC were grown on microscopy coverslips and were subsequently incubated with Vanco-800CW. Images recorded by fluorescence microscopy reveal binding of Vanco-800CW (red) to the Gram-positive bacterial biofilms (*S. aureus* and *S. epidermidis* ATCC) but not to the Gram-negative bacteria (*E. coli* ATTC). (b) *S. epidermidis* ATCC was further selected to investigate the binding of Vanco-FL-800CW. Vanco-FL-800CW was also able to bind to *S. epidermidis* ATCC and the BODIPY-FL signal (green) colocalized with the 800CW signal (red). The colocalization is presented in yellow. Scale bars: 40 μm.

spectra recorded on an HPLC system with photodiode array (PDA) detection (Figure 5). To determine whether the binding of vancomycin to Gram-positive bacteria was affected upon dual labeling, biofilms of *S. epidermidis* ATCC were incubated with Vanco-FL-800CW and images were acquired with a fluorescence microscope, as performed before for Vanco-800CW. As shown in Figure 4b, Vanco-FL-800CW is capable of binding to *S. epidermidis* ATCC and the fluorescence signals from BODIPY-FL and 800CW colocalize with the bacteria. With the successful preparation of this new molecule, we not only broadened the potential applicability of vancomycin as a dual-imaging targeting probe but also supported our findings regarding the molecular structure of Vanco-800CW (Figure 3) since IRdye800CW was successfully coupled to the free secondary amine of Vanco-FL under the optimized conditions.

Inspired by the positive results for the synthesis and purification of compounds **1** and **2**, we further investigated the scope of the established synthetic method. First, we explored the possibility of using a different targeting agent, namely, amphotericin B, to provide an optical imaging agent for fungal infections.[46,47] Amphotericin B binds to ergosterol, which is abundant only in the cell membrane of fungi.[48] We were pleased to discover that the optimized reaction conditions successfully yield compound **3** (Ampho-800CW; Figure 1). After purification by semipreparative HPLC, the purity and identity were confirmed by UPLC-MS and UV−vis analysis (Figure 5). Since amphotericin B only contains one amine functionality as a possible coupling site, the fragmentation analysis by HRMS was omitted.

Next, we explored the generality of the synthetic method with respect to different dyes by applying the conditions optimized for compound **1** for the conjugation of vancomycin to the NHS ester of IRdye700DX, an NIR dye that simultaneously functions as a photosensitizer, enabling its application for antimicrobial photodynamic therapy.[49,50] Also in this case, the desired product (**4**, Vanco-700DX; Figure 1) was obtained and could be purified in the same way, as described for Vanco-800CW. Subsequently, the product was analyzed by UPLC-MS and UV−vis spectrometry to confirm the purity and identity (Figure 5). High-resolution tandem mass spectrometry indicates that, also, this dye couples to the secondary amine at the *N*-terminus of vancomycin (Figure S16). To investigate whether the ability of IRDye700DX to produce reactive oxygen species (more specifically, singlet oxygen [$^1O_2$]) was affected upon conjugation to vancomycin, a detection method based on 1,3-diphenylisobenzofuran (DPBF) was applied (see the Supporting Information, Figure

https://dx.doi.org/10.1021/acsomega.0c02094
ACS Omega 2020, 5, 22071−22080

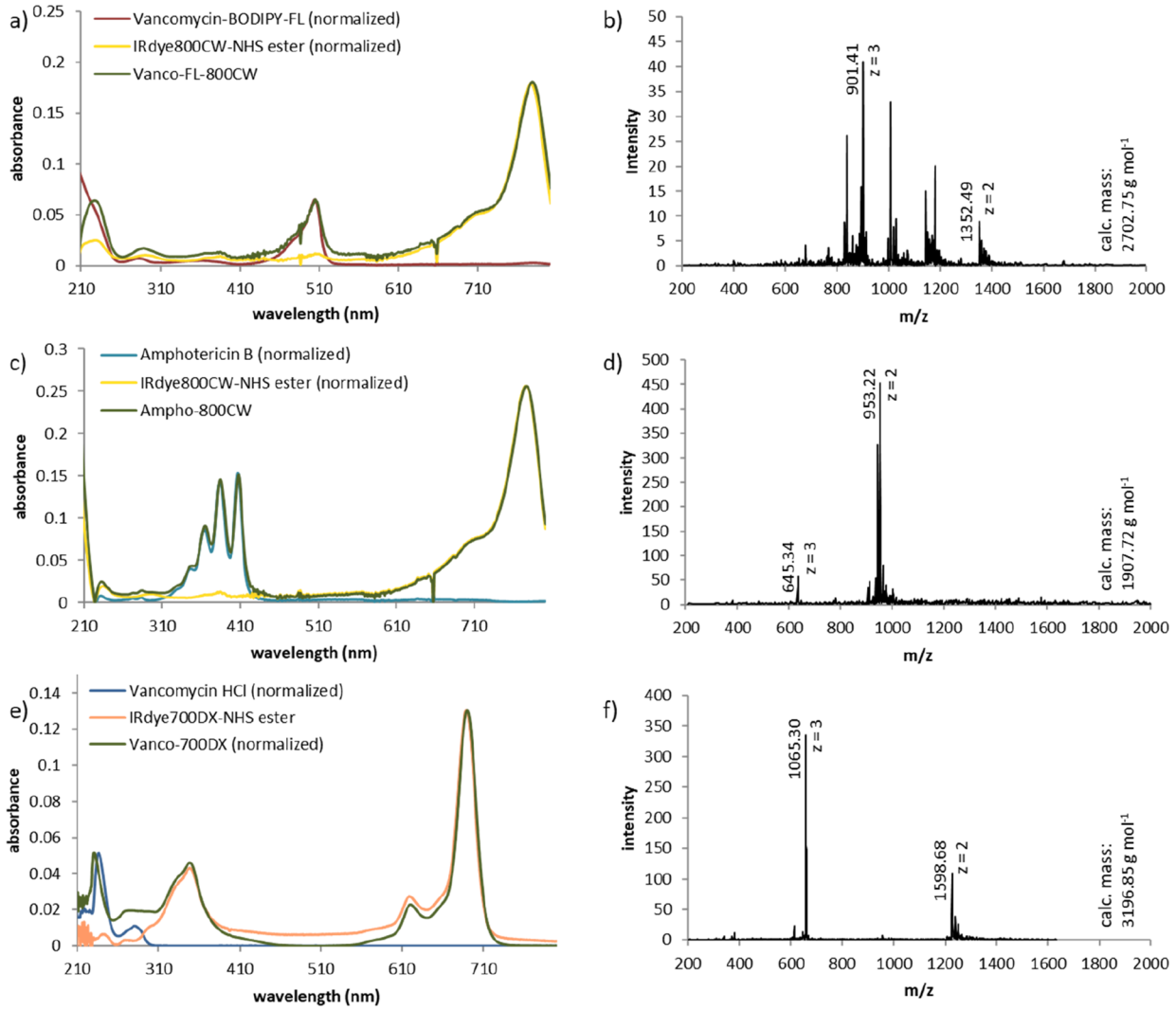

Figure 5. Analytical data for (a, b) Vanco-FL-800CW **2**, (c, d) Ampho-800CW **3**, and (e, f) Vanco-700DX **4**. (a) Overlay of the PDA spectra of HPLC peaks corresponding to Vanco-FL (red), IRdye800CW-NHS ester (yellow), and Vanco-FL-800CW (green). (b) Mass spectrum of the product peak (Figure S9) recorded on a UPLC-MS device. (c) Overlay of PDA spectra of the HPLC peak corresponding to amphotericin B (blue), IRdye800CW NHS ester (yellow), and Ampho-800CW (green). (d) Mass spectrum of the product peak (Figure S10) recorded on a UPLC-MS device. (e) Overlay of the UV−vis absorption spectra of vancomycin (blue), IRdye700DX-NHS ester (orange), and Vanco-700DX (green). The spectra were obtained of the pure samples in 1% DMSO in water on a UV−vis spectrophotometer. (f) Mass spectrum of the product peak (Figure S11) recorded on a UPLC-MS device.

S18). DPBF is photo-oxidized by $^1O_2$, and its absorbance decay can be monitored by UV−vis spectrophotometry at 415 nm. Irradiation of both IRDye700DX and Vanco-700DX for 70 s with a high output LED device that emits light at 690 nm,[51] at an irradiance of 10 mW cm^{-2}, resulted in complete photo-oxidation of the DPBF (initial concentration: 100 μM) at similar rates.

The conformational changes that vancomycin might undergo upon labeling with one or two dyes did not impair its ability to bind to bacteria, as demonstrated using biofilms grown *in vitro* (Figure 4). However, the conjugation can affect its antimicrobial activity since IRDye800CW and IRDye700DX bind to the secondary amine of *N*-methyl-leucine, which is an important amino acid in the binding to the target dipeptide D-Ala-D-Ala in the bacterial cell wall, thereby influencing the antimicrobial properties of vancomycin.[52] Thus, the minimum inhibitory concentrations (MIC) of vancomycin, Vanco-800CW, and Vanco-700DX against an *S. epidermidis* strain were assessed in liquid cultures by testing serial dilutions and by antibiotic disk diffusion assays on agar plates (Supporting Information, Figure S19). The MIC of vancomycin toward *S. epidermidis* was 2 mg/L, while the MIC of both conjugates was higher than 8 mg/L (Figure S19). Moreover, 5 μg of diffusion discs placed on sample agar plates showed no inhibition of bacterial growth around the discs for Vanco-800CW and Vanco-700DX (Figure S19e). The loss of antimicrobial activity upon conjugation probably relates to a lowered affinity for the D-Ala-D-Ala dipeptide when compared to the unlabeled vancomycin. Importantly, we regard the absence of antimicrobial activity as beneficial from a microbiological viewpoint because this makes it less likely that the repeated usage of the conjugates will elicit resistance to vancomycin.

CONCLUSIONS

In conclusion, we established an efficient, transferable, and reproducible method for the synthesis and purification of conjugates of near-infrared dyes that can potentially be used

https://dx.doi.org/10.1021/acsomega.0c02094
ACS Omega 2020, 5, 22071−22080

for the imaging and treatment of bacterial and fungal infections. The reported research fulfils the need for selective methods to synthesize adducts of highly functionalized small molecules with relevant dyes used in medical imaging. It may substantially facilitate the development of new optical imaging agents since it offers a straightforward procedure that can be repeated also in laboratories that are not dedicated to organic synthesis.

EXPERIMENTAL SECTION

Optimized Procedure for the Synthesis of Compound 1 (Vanco-800CW Conjugate). Vancomycin hydrochloride (100 mg/mL in DMSO, 146 μL, 10 μmol), HBTU (25.5 mg/mL in DMSO, 57.6 μL, 3.9 μmol, or equimolar amount of HATU), DIPEA (22.5 mg/mL in DMSO, 57.3 μL, 10 μmol), and IRdye800CW-NHS ester (5 mg/mL in DMSO, 180 μL, 0.8 μmol) were mixed and left at room temperature overnight. Subsequently, H_2O (2.6 mL) was added to the reaction mixture and the suspension was centrifuged for 10 min at rcf = 16.9 × 1000*g*. The supernatant was centrifuged again, and the combined pellets were redissolved in a mixture of DMSO, acetonitrile, and H_2O for purification by semipreparative HPLC (elution gradient from 10 to 70% organic phase).

ASSOCIATED CONTENT

Supporting Information

The Supporting Information is available free of charge at https://pubs.acs.org/doi/10.1021/acsomega.0c02094.

Synthetic procedures, HPLC traces for the reaction monitoring, UPLC-MS and HRMS data for final products and biological evaluation procedures, and the determination of singlet oxygen production and MIC values (PDF)

AUTHOR INFORMATION

Corresponding Author

Wiktor Szymański − *Department of Radiology, Medical Imaging Center, University of Groningen, University Medical Center Groningen, Groningen 9713GZ, The Netherlands; Stratingh Institute for Chemistry, University of Groningen, Groningen 9747 AG, The Netherlands;* orcid.org/0000-0002-9754-9248; Email: w.szymanski@umcg.nl

Authors

Friederike Reeßing − *Department of Radiology, Medical Imaging Center, University of Groningen, University Medical Center Groningen, Groningen 9713GZ, The Netherlands; Stratingh Institute for Chemistry, University of Groningen, Groningen 9747 AG, The Netherlands*

Mafalda Bispo − *Department of Medical Microbiology, University of Groningen, University Medical Center Groningen, Groningen 9713GZ, The Netherlands*

Marina López-Álvarez − *Department of Medical Microbiology, University of Groningen, University Medical Center Groningen, Groningen 9713GZ, The Netherlands*

Marleen van Oosten − *Department of Medical Microbiology, University of Groningen, University Medical Center Groningen, Groningen 9713GZ, The Netherlands*

Ben L. Feringa − *Department of Radiology, Medical Imaging Center, University of Groningen, University Medical Center Groningen, Groningen 9713GZ, The Netherlands; Stratingh Institute for Chemistry, University of Groningen, Groningen 9747 AG, The Netherlands;* orcid.org/0000-0003-0588-8435

Jan Maarten van Dijl − *Department of Medical Microbiology, University of Groningen, University Medical Center Groningen, Groningen 9713GZ, The Netherlands;* orcid.org/0000-0002-5688-8438

Complete contact information is available at: https://pubs.acs.org/10.1021/acsomega.0c02094

Notes

The authors declare no competing financial interest.

ACKNOWLEDGMENTS

We gratefully acknowledge M.D. Linssen for providing the IRdye800CW-NHS ester. We thank J.L. Sneep and M.P. de Vries for analytical support. This research was supported by the Dutch Organization for Scientific Research, NWO VIDI grant no. 723.014.001 for W.S. M.B. and M.L.-A acknowledge the EU Horizon 2020 programs under the Marie Skłodowska-Curie grant agreement 713660 (Pronkjewail).

REFERENCES

(1) Pysz, M. A.; Gambhir, S. S.; Willmann, J. K. Molecular Imaging: Current Status and Emerging Strategies. *Clin. Radiol.* **2010**, *65*, 500−516.

(2) Hoffman, J. M.; Gambhir, S. S. Molecular Imaging: The Vision and Opportunity for Radiology in the Future. *Radiology* **2007**, *244*, 39−47.

(3) Sosnovik, D. E.; Weissleder, R. Emerging Concepts in Molecular MRI. *Curr. Opin. Biotechnol.* **2007**, *18*, 4−10.

(4) Rao, J.; Dragulescu-Andrasi, A.; Yao, H. Fluorescence Imaging in Vivo: Recent Advances. *Curr. Opin. Biotechnol.* **2007**, *18*, 17−25.

(5) Hong, G.; Antaris, A. L.; Dai, H. Near-Infrared Fluorophores for Biomedical Imaging. *Nat. Biomed. Eng.* **2017**, *1*, 0010.

(6) Haque, A.; Faizi, M. S. H.; Rather, J. A.; Khan, M. S. Next Generation NIR Fluorophores for Tumor Imaging and Fluorescence-Guided Surgery: A Review. *Bioorg. Med. Chem.* **2017**, *25*, 2017−2034.

(7) Koch, M.; Symvoulidis, P.; Ntziachristos, V. Tackling Standardization in Fluorescence Molecular Imaging. *Nat. Photonics* **2018**, *12*, 505−515.

(8) Ntziachristos, V. Going Deeper than Microscopy: The Optical Imaging Frontier in Biology. *Nat. Methods* **2010**, *7*, 603−614.

(9) Olson, M. T.; Ly, Q. P.; Mohs, A. M. Fluorescence Guidance in Surgical Oncology: Challenges, Opportunities, and Translation. *Mol. Imaging Biol.* **2019**, *21*, 200−218.

(10) van Dam, G. M.; Themelis, G.; Crane, L. M. A.; Harlaar, N. J.; Pleijhuis, R. G.; Kelder, W.; Sarantopoulos, A.; de Jong, J. S.; Arts, H. J. G.; van der Zee, A. G. J.; Bart, J.; Low, P. S.; Ntziachristos, V. Intraoperative Tumor-Specific Fluorescence Imaging in Ovarian Cancer by Folate Receptor-α Targeting: First in-Human Results. *Nat. Med.* **2011**, *17*, 1315−1319.

(11) Miller, S. E.; Tummers, W. S.; Teraphongphom, N.; van den Berg, N. S.; Hasan, A.; Ertsey, R. D.; Nagpal, S.; Recht, L. D.; Plowey, E. D.; Vogel, H.; Harsh, G. R.; Grant, G. A.; Li, G. H.; Rosenthal, E. L. First-in-Human Intraoperative near-Infrared Fluorescence Imaging of Glioblastoma Using Cetuximab-IRDye800. *J. Neuro-Oncol.* **2018**, *139*, 135−143.

(12) Hameed, S.; Dai, Z. Near-Infrared Fluorescence Probes for Surgical Navigation. *Mater. Today Chem.* **2018**, *10*, 90−103.

(13) van den Bos, J.; van Kooten, L.; Engelen, S. M. E.; Lubbers, T.; Stassen, L. P. S.; Bouvy, N. D. Feasibility of Indocyanine Green Fluorescence Imaging for Intraoperative Identification of Parathyroid Glands during Thyroid Surgery. *Head Neck* **2018**, *41*, 340−348.

(14) Burggraaf, J.; Kamerling, I. M. C.; Gordon, P. B.; Schrier, L.; de Kam, M. L.; Kales, A. J.; Bendiksen, R.; Indrevoll, B.; Bjerke, R. M.; Moestue, S. A.; Yazdanfar, S.; Langers, A. M. J.; Swaerd-Nordmo, M.;

Torheim, G.; Warren, M. V.; Morreau, H.; Voorneveld, P. W.; Buckle, T.; van Leeuwen, F. W. B.; Ødegårdstuen, L.-I.; Dalsgaard, G. T.; Healey, A.; Hardwick, J. C. H. Detection of Colorectal Polyps in Humans Using an Intravenously Administered Fluorescent Peptide Targeted against C-Met. *Nat. Med.* **2015**, *21*, 955−961.
(15) van der Sommen, F.; Curvers, W. L.; Nagengast, W. B. Novel Developments in Endoscopic Mucosal Imaging. *Gastroenterology* **2018**, *154*, 1876−1886.
(16) Nagengast, W. B.; Hartmans, E.; Garcia-Allende, P. B.; Peters, F. T. M.; Linssen, M. D.; Koch, M.; Koller, M.; Tjalma, J. J. J.; Karrenbeld, A.; Jorritsma-Smit, A.; Kleibeuker, J. H.; van Dam, G. M.; Ntziachristos, V. Near-Infrared Fluorescence Molecular Endoscopy Detects Dysplastic Oesophageal Lesions Using Topical and Systemic Tracer of Vascular Endothelial Growth Factor A. *Gut* **2019**, *68*, 7−10.
(17) Gao, R. W.; Teraphongphom, N. T.; van den Berg, N. S.; Martin, B. A.; Oberhelman, N. J.; Divi, V.; Kaplan, M. J.; Hong, S. S.; Lu, G.; Ertsey, R.; Tummers, W. S. F. J.; Gomez, A. J.; Holsinger, F. C.; Kong, C. S.; Colevas, A. D.; Warram, J. M.; Rosenthal, E. L. Determination of Tumor Margins with Surgical Specimen Mapping Using Near-Infrared Fluorescence. *Cancer Res.* **2018**, *78*, 5144−5154.
(18) Kobayashi, H.; Choyke, P. L. Target-Cancer-Cell-Specific Activatable Fluorescence Imaging Probes: Rational Design and in Vivo Applications. *Acc. Chem. Res.* **2011**, *44*, 83−90.
(19) Koller, M.; Qiu, S.-Q.; Linssen, M. D.; Jansen, L.; Kelder, W.; de Vries, J.; Kruithof, I.; Zhang, G.-J.; Robinson, D. J.; Nagengast, W. B.; Jorritsma-Smit, A.; van der Vegt, B.; van Dam, G. M. Implementation and Benchmarking of a Novel Analytical Framework to Clinically Evaluate Tumor-Specific Fluorescent Tracers. *Nat. Commun.* **2018**, *9*, 3739.
(20) van Manen, L.; Handgraaf, H. J. M.; Diana, M.; Dijkstra, J.; Ishizawa, T.; Vahrmeijer, A. L.; Mieog, J. S. D. A Practical Guide for the Use of Indocyanine Green and Methylene Blue in Fluorescence-Guided Abdominal Surgery. *J. Surg. Oncol.* **2018**, *118*, 283−300.
(21) Atreya, R.; Neumann, H.; Neufert, C.; Waldner, M. J.; Billmeier, U.; Zopf, Y.; Willma, M.; App, C.; Münster, T.; Kessler, H.; Maas, S.; Gebhardt, B.; Heimke-Brinck, R.; Reuter, E.; Dörje, F.; Rau, T. T.; Uter, W.; Wang, T. D.; Kiesslich, R.; Vieth, M.; Hannappel, E.; Neurath, M. F. In Vivo Imaging Using Fluorescent Antibodies to Tumor Necrosis Factor Predicts Therapeutic Response in Crohn's Disease. *Nat. Med.* **2014**, *20*, 313−318.
(22) Sturm, M. B.; Joshi, B. P.; Lu, S.; Piraka, C.; Khondee, S.; Elmunzer, B. J.; Kwon, R. S.; Beer, D. G.; Appelman, H. D.; Turgeon, D. K.; Wang, T. D. Targeted Imaging of Esophageal Neoplasia with a Fluorescently Labeled Peptide: First-in-Human Results. *Sci. Transl. Med.* **2013**, *5*, 184ra61.
(23) van Scheltinga, A. G. T. T.; van Dam, G. M.; Nagengast, W. B.; Ntziachristos, V.; Hollema, H.; Herek, J. L.; Schröder, C. P.; Kosterink, J. G. W.; Lub-de Hoog, M. N.; de Vries, E. G. E. Intraoperative Near-Infrared Fluorescence Tumor Imaging with Vascular Endothelial Growth Factor and Human Epidermal Growth Factor Receptor 2 Targeting Antibodies. *J. Nucl. Med.* **2011**, *52*, 1778−1785.
(24) Srinivasarao, M.; Galliford, C. V.; Low, P. S. Principles in the Design of Ligand-Targeted Cancer Therapeutics and Imaging Agents. *Nat. Rev. Drug Discovery* **2015**, *14*, 203−219.
(25) Harlaar, N. J.; Koller, M.; de Jongh, S. J.; van Leeuwen, B. L.; Hemmer, P. H.; Kruijff, S.; van Ginkel, R. J.; Been, L. B.; de Jong, J. S.; Kats-Ugurlu, G.; Linssen, M. D.; Jorritsma-Smit, A.; van Oosten, M.; Nagengast, W. B.; Ntziachristos, V.; van Dam, G. M. Molecular Fluorescence-Guided Surgery of Peritoneal Carcinomatosis of Colorectal Origin: A Single-Centre Feasibility Study. *Lancet Gastroenterol. Hepatol.* **2016**, *1*, 283−290.
(26) Kijanka, M.; Warnders, F.-J.; el Khattabi, M.; Lub-De Hooge, M.; van Dam, G. M.; Ntziachristos, V.; de Vries, L.; Oliveira, S.; van Bergen En Henegouwen, P. M. P. Rapid Optical Imaging of Human Breast Tumour Xenografts Using Anti-HER2 VHHs Site-Directly Conjugated to IRDye 800CW for Image-Guided Surgery. *Eur. J. Nucl. Med. Mol. Imaging* **2013**, *40*, 1718−1729.
(27) Korb, M. L.; Hartman, Y. E.; Kovar, J.; Zinn, K. R.; Bland, K. I.; Rosenthal, E. L. Use of Monoclonal Antibody-IRDye800CW Bioconjugates in the Resection of Breast Cancer. *J. Surg. Res.* **2014**, *188*, 119−128.
(28) Muselaers, C. H. J.; Stillebroer, A. B.; Rijpkema, M.; Franssen, G. M.; Oosterwijk, E.; Mulders, P. F. A.; Oyen, W. J. G.; Boerman, O. C. Optical Imaging of Renal Cell Carcinoma with Anti-Carbonic Anhydrase IX Monoclonal Antibody Girentuximab. *J. Nucl. Med.* **2014**, *55*, 1035−1040.
(29) Rosenthal, E. L.; Warram, J. M.; de Boer, E.; Chung, T. K.; Korb, M. L.; Brandwein-Gensler, M.; Strong, T. V.; Schmalbach, C. E.; Morlandt, A. B.; Agarwal, G.; Hartman, Y. E.; Carroll, W. R.; Richman, J. S.; Clemons, L. K.; Nabell, L. M.; Zinn, K. R. Safety and Tumor Specificity of Cetuximab-IRDye800 for Surgical Navigation in Head and Neck Cancer. *Clin. Cancer Res.* **2015**, *21*, 3658−3666.
(30) Heath, C. H.; Deep, N. L.; Beck, L. N.; Day, K. E.; Sweeny, L.; Zinn, K. R.; Huang, C. C.; Rosenthal, E. L. Use of Panitumumab-IRDye800 to Image Cutaneous Head and Neck Cancer in Mice. *Otolaryngol.–Head Neck Surg.* **2013**, *148*, 982−990.
(31) Adams, K. E.; Ke, S.; Kwon, S.; Liang, F.; Fan, Z.; Lu, Y.; Hirschi, K.; Mawad, M. E.; Barry, M. A.; Sevick-Muraca, E. M. Comparison of Visible and Near-Infrared Wavelength-Excitable Fluorescent Dyes for Molecular Imaging of Cancer. *J. Biomed. Opt.* **2007**, *12*, No. 024017.
(32) Sun, C.; Du, W.; Wang, B.; Dong, B.; Wang, B. Research progress of near-infrared fluorescence probes based on indole heptamethine cyanine dyes in vivo and in vitro. *BMC Chem.* **2020**, *14*, 21.
(33) Tang, C.; Du, Y.; Liang, Q.; Cheng, Z.; Tian, J. Development of a Novel Histone Deacetylase-Targeted Near-Infrared Probe for Hepatocellular Carcinoma Imaging and Fluorescence Image-Guided Surgery. *Mol. Imaging Biol.* **2020**, *22*, 476−485.
(34) Kovar, J. L.; Volchek, W.; Sevick-Muraca, E.; Simpson, M. A.; Olive, D. M. Characterization and performance of a near-infrared 2-deoxyglucose optical imaging agent for mouse cancer models. *Anal. Biochem.* **2008**, *384*, 254−262.
(35) Li, D.; Zhang, J.; Chi, C.; Xiao, X.; Wang, J.; Lang, L.; Ali, I.; Niu, G.; Zhang, L.; Tian, J.; Ji, N.; Zhu, Z.; Chen, X. First-in-human study of PET and optical dual-modality image-guided surgery in glioblastoma using 68Ga-IRDye800CW-BBN. *Theranostics* **2018**, *8*, 2508−2520.
(36) Baranski, A.-C.; Schäfer, M.; Bauder-Wüst, U.; Roscher, M.; Schmidt, J.; Stenau, E.; Simpfendörfer, T.; Teber, D.; Maier-Hein, L.; Hadaschik, B.; Haberkorn, U.; Eder, M.; Kopka, K. PSMA-11−Derived Dual-Labeled PSMA Inhibitors for Preoperative PET Imaging and Precise Fluorescence-Guided Surgery of Prostate Cancer. *J. Nucl. Med.* **2018**, *59*, 639−645.
(37) Duan, X.; Liu, F.; Kwon, H.; Byun, Y.; Minn, I.; Cai, X.; Zhang, J.; Pomper, M. G.; Yang, Z.; Xi, Z.; Yang, X. (*S*)-3-(Carboxyformamido)-2-(3-(carboxymethyl)ureido)propanoic Acid as a Novel PSMA Targeting Scaffold for Prostate Cancer Imaging. *J. Med. Chem.* **2020**, *63*, 3563−3576.
(38) Gao, Z.; Li, G.; Li, X.; Zhou, J.; Duan, X.; Chen, J.; Joshi, B. P.; Kuick, R.; Khoury, B.; Thomas, D. G.; Fields, T.; Sabel, M. S.; Appelman, H. D.; Zhou, Q.; Li, H.; Kozloff, K.; Wang, T. D. In vivo near-infrared imaging of ErbB2 expressing breast tumors with dual-axes confocal endomicroscopy using a targeted peptide. *Sci. Rep.* **2017**, *7*, 14404.
(39) van Oosten, M.; Schäfer, T.; Gazendam, J. A. C.; Ohlsen, K.; Tsompanidou, E.; de Goffau, M. C.; Harmsen, H. J. M.; Crane, L. M. A.; Lim, E.; Francis, K. P.; Cheung, L.; Olive, M.; Ntziachristos, V.; van Dijl, J. M.; van Dam, G. M. Real-Time in Vivo Imaging of Invasive- and Biomaterial-Associated Bacterial Infections Using Fluorescently Labelled Vancomycin. *Nat. Commun.* **2013**, *4*, 2584.
(40) ter Weele, E. J.; Van Scheltinga, A. G. T. T.; Linssen, M. D.; Nagengast, W. B.; Lindner, I.; Jorritsma-Smit, A.; de Vries, E. G. E.; Kosterink, J. G. W.; Lub-De Hooge, M. N. Development, Preclinical Safety, Formulation, and Stability of Clinical Grade Bevacizumab-

https://dx.doi.org/10.1021/acsomega.0c02094
ACS Omega 2020, 5, 22071−22080

800CW, a New near Infrared Fluorescent Imaging Agent for First in Human Use. *Eur. J. Pharm. Biopharm.* **2016**, *104*, 226−234.
(41) Valeur, E.; Bradley, M. Amide Bond Formation: Beyond the Myth of Coupling Reagents. *Chem. Soc. Rev.* **2009**, *38*, 606−631.
(42) Kannan, R.; Harris, C. M.; Harris, T. M.; Waltho, J. P.; Skelton, N. J.; Williams, D. H. Function of the Amino Sugar and *N*-Terminal Amino Acid of the Antibiotic Vancomycin in Its Complexation with Cell Wall Peptides. *J. Am. Chem. Soc.* **1988**, *110*, 2946−2953.
(43) Kailemia, M. J.; Ruhaak, L. R.; Lebrilla, C. B.; Amster, I. J. Oligosaccharide Analysis by Mass Spectrometry: A Review of Recent Developments. *Anal. Chem.* **2014**, *86*, 196−212.
(44) Staroske, T.; Williams, D. H. Synthesis of Covalent Head-to-Tail Dimers of Vancomycin. *Tetrahedron Lett.* **1998**, *39*, 4917−4920.
(45) Yang, C.; Ren, C.; Zhou, J.; Liu, J.; Zhang, Y.; Huang, F.; Ding, D.; Xu, B.; Liu, J. Dual Fluorescent- and Isotopic-Labelled Self-Assembling Vancomycin for *in vivo* Imaging of Bacterial Infections. *Angew. Chem., Int. Ed.* **2017**, *56*, 2356−2360.
(46) Van Dyck, K.; Rogiers, O.; Vande Velde, G.; Van Dijck, P. Let's shine a light on fungal infections: A noninvasive imaging toolbox. *PLoS Pathog.* **2020**, *16*, No. e1008257.
(47) Petrik, M.; Pfister, J.; Misslinger, M.; Decristoforo, C.; Haas, H. Siderophore-Based Molecular Imaging of Fungal and Bacterial Infections—Current Status and Future Perspectives. *J. Fungi* **2020**, *6*, 73.
(48) Gray, K. C.; Palacios, D. S.; Dailey, I.; Endo, M. M.; Uno, B. E.; Wilcock, B. C.; Burke, M. D. Amphotericin Primarily Kills Yeast by Simply Binding Ergosterol. *Proc. Natl. Acad. Sci. U. S. A.* **2012**, *109*, 2234−2239.
(49) Hu, X.; Huang, Y.-Y.; Wang, Y.; Wang, X.; Hamblin, M. R. Antimicrobial Photodynamic Therapy to Control Clinically Relevant Biofilm Infections. *Front. Microbiol.* **2018**, *9*, 1299.
(50) Cieplik, F.; Deng, D.; Crielaard, W.; Buchalla, W.; Hellwig, E.; Al-Ahmad, A.; Maisch, T. Antimicrobial photodynamic therapy − what we know and what we don't. *Crit. Rev. Microbiol.* **2018**, *44*, 571−589.
(51) de Boer, E.; Warram, J. M.; Hartmans, E.; Bremer, P. J.; Bijl, B.; Crane, L. M. A.; Nagengast, W. B.; Rosenthal, E. L.; van Dam, G. M. A Standardized Light-Emitting Diode Device for Photoimmunotherapy. *J. Nucl. Med.* **2014**, *55*, 1893−1898.
(52) Wang, F.; Zhou, H.; Olademehin, O. P.; Kim, S. J.; Tao, P. Insights into Key Interactions between Vancomycin and Bacterial Cell Wall Structures. *ACS Omega* **2018**, *3*, 37−45.

https://dx.doi.org/10.1021/acsomega.0c02094
ACS Omega 2020, 5, 22071−22080